

**THERMAL BEHAVIORS AND IONIC CONDUCTIVITY OF
COMPOSITE ENR-50-BASED POLYMER ELECTROLYTES**

by

TAN WEI LENG

**Thesis submitted in fulfillment of the requirements
for the degree of
Doctor of Philosophy**

February 2013

ACKNOWLEDGEMENTS

I would like to take this opportunity to extend my heartiest appreciation to many people who have made it possible for me to complete this thesis.

First of all, I would like to express my appreciation to my supervisor, Prof. Mohamad Abu Bakar for his tremendous guidance, advice, encouragement and support throughout the completion of this work.

My sincere gratitude also goes to our helpful and dedicated lab assistants and staffs – Mr. Ali, Mr. Kamarulazwan, Mr. Burhanudin, Mrs. Ami Mardiana and Mrs. Saripah Mansur from School of Chemical Sciences, Ms. Jamilah, Mr. Johari, Mrs. Faizah and Mr. Masrul from the Electron Microscopy Unit, School of Biological Sciences as well as Mr. Karunakaran and Mr. Mohamed Mustaqim from School of Physics.

A special thanks to Mr. Kan and Ms. Fiona Lau from ASEPTec Sdn. Bhd. for their kindness assistance and consistence help in accomplishing this work.

I would also like to acknowledge the financial support from Universiti Sains Malaysia for the awarded PRGS grant 1001/PKIMIA/843032 and USM Fellowship.

Last but not least, my heartfelt appreciation goes to my friends and beloved family, who have assisted me in various aspects and given me an everlasting support. Thank you.

TAN WEI LENG

December 2012

TABLE OF CONTENTS

	Page
Acknowledgements	ii
Table of Contents	iii
List of Tables	viii
List of Figures	x
List of Symbols	xiv
List of Abbreviations	xv
Abstrak	xviii
Abstract	xx
CHAPTER 1 – INTRODUCTION	
1.1 A Brief Overview	1
1.2 Problem Statements	1
1.3 Research Aim and Objectives	3
1.4 Scope of Study	3
1.5 Thesis Layout	4
1.6 References	5
CHAPTER 2 - LITERATURE REVIEW	
2.1 Polymer Electrolytes	6
2.1.1 Salts	6
2.1.2 Polymer Hosts	8
2.1.3 Additives	12
2.1.3.1 Organic Plasticizers	12
2.1.3.2 Fillers	12
2.1.3.3 Iodine Dopant	14
2.2 Application of Polymer Electrolytes	15
2.3 Epoxidized Natural Rubber	16
2.3.1 ENR Blends	17
2.3.2 Inorganic/ENR Composites	17
2.3.3 ENR-based Polymer Electrolytes	18
2.4 Iron Oxides	18
2.4.1 Magnetite	19
2.4.2 Application of Magnetite	21
2.5 Kinetic Analyses	22

2.5.1	Theoretical Background	22
2.5.2	Isoconversional Methods	23
2.5.2.1	Kissinger Method	23
2.5.2.2	Flynn-Wall-Ozawa Method	24
2.5.3	Model-fitting Methods	24
2.5.3.1	Coats and Redfern Method	24
2.5.3.2	Criado Method	25
2.6	References	27

CHAPTER 3 – EXPERIMENTAL

3.1	Materials	39
3.2	Methods	39
3.2.1	Preparation of Salt-ENR-50 Polymer Electrolytes	39
3.2.1.1	Effect of anion of the LiX salts	39
3.2.1.2	Effect of cation of the MI salts	40
3.2.2	Preparation of Fe ₃ O ₄ /ENR-50 Nanocomposites	41
3.2.3	Preparation of LiX-Fe ₃ O ₄ /ENR-50 Composite Polymer Electrolytes	42
3.3	Characterization Techniques	43
3.3.1	Transmission Electron Microscopy	43
3.3.2	Scanning Electron Microscopy/X-mapping	44
3.3.3	Fourier Transform Infrared Spectroscopy	44
3.3.4	Powder X-ray Diffraction Technique	44
3.3.5	Atomic Absorption Spectroscopy	44
3.3.6	Differential Scanning Calorimetry	45
3.3.7	Thermogravimetric Analysis	45
3.3.8	Electrochemical Impedance Spectroscopy	45
3.4	Kinetic Studies	46
3.4.1	Determination of Activation Energy	46
3.4.1.1	Kissinger Method	46
3.4.1.2	Flynn-Wall-Ozawa method	47
3.4.2	Determination of Degradation Model	47
3.4.2.1	Coats and Redfern Method	47
3.4.2.2	Criado Method	48
3.5	References	49

**CHAPTER 4 – BINARY SALT-EPOXIDIZED NATURAL RUBBER
POLYMER ELECTROLYTES: SYNTHESIS,
CHARACTERIZATION, THERMAL AND ELECTRICAL
PROPERTIES**

4.1	Effect of Anion of Lithium Salt in LiX-ENR-50 PEs	50
4.1.1	Preparation of LiX-ENR-50 Polymer Electrolytes	50
4.1.2	Characterization	51
4.1.2.1	Scanning Electron Microscopy/X-mapping	51
4.1.2.2	Fourier Transform Infrared Spectroscopy	54
4.1.3	Thermal Properties	58
4.1.3.1	Differential Scanning Calorimetry	58
4.1.3.2	Thermogravimetric Analysis	62
4.1.4	Conductivity of LiX-ENR-50 PEs	66
4.1.4.1	Electrochemical Impedance Spectroscopy	66
4.2	Effect of Cation of Iodide Salt in MI-ENR-50 PEs	70
4.2.1	Preparation of MI-ENR-50 Polymer Electrolytes	70
4.2.2	Characterization	70
4.2.2.1	Differential Scanning Calorimetry	70
4.2.2.2	Fourier Transform Infrared Spectroscopy	71
4.2.2.3	Scanning Electron Microscopy/X-mapping	73
4.2.3	Thermal Properties	77
4.2.3.1	Thermogravimetric Analysis	77
4.2.4	Conductivity	80
4.2.4.1	Electrochemical Impedance Spectroscopy	80
4.3	Summary	82
4.4	References	85

**CHAPTER 5 – THERMAL DEGRADATION OF BINARY SALT-
EPOXIDIZED NATURAL RUBBER POLYMER
ELECTROLYTES**

5.1	Purified ENR-50	87
5.2	LiX-ENR-50 PEs	93
5.3	MI-ENR-50 PEs	102
5.4	Summary	110
5.5	References	112

**CHAPTER 6 – MAGNETITE/EPOXIDIZED NATURAL RUBBER
NANOCOMPOSITES: SYNTHESIS,
CHARACTERIZATION, THERMAL AND ELECTRICAL
PROPERTIES**

6.1	Synthesis and Characterization	113
	6.1.1 Powder X-ray Diffraction	113
	6.1.2 Fourier Transform Infrared Spectroscopy	114
	6.1.3 Scanning Electron Microscopy/X-mapping and Transmission Electron Microscopy	117
6.2	Thermal Properties	121
	6.2.1 Differential Scanning Calorimetry	121
	6.2.2 Thermogravimetric Analysis	123
6.3	Conductivity	126
	6.3.1 Electrochemical Impedance Spectroscopy	126
6.4	Summary	131
6.5	References	133

**CHAPTER 7 – LITHIUM SALT-MAGNETITE/EPOXIDIZED NATURAL
RUBBER COMPOSITE POLYMER ELECTROLYTES:
SYNTHESIS, CHARACTERIZATION, THERMAL AND
ELECTRICAL PROPERTIES**

7.1	Synthesis and Characterization	136
	7.1.1 Fourier Transform Infrared Spectroscopy	136
	7.1.2 Scanning Electron Microscopy/X-mapping	140
	7.1.3 Transmission Electron Microscopy	143
7.2	Thermal Properties	145
	7.2.1 Differential Scanning Calorimetry	145
	7.2.2 Thermogravimetric Analysis	146
7.3	Conductivity	150
	7.3.1 Electrochemical Impedance Spectroscopy	150
7.4	Summary	155
7.5	References	157

CHAPTER 8 – THERMAL DEGRADATION OF		
MAGNETITE/EPOXIDIZED NATURAL RUBBER		
COMPOSITE AND SALT-MAGNETITE/EPOXIDIZED		
NATURAL RUBBER COMPOSITE POLYMER		
ELECTROLYTES		
8.1	Fe ₃ O ₄ /ENR-50 Base Composite	158
8.2	LiX- Fe ₃ O ₄ /ENR-50 CPEs	166
8.3	Summary	174
8.4	References	175
CHAPTER 9 – CONCLUSIONS		
9.1	Conclusions	176
9.2	Recommendation for Future Work	177
	List of Publications and Presentations	178

LIST OF TABLES

	Page
Table 2.1 Lithium salts in PEO-based PE systems	7
Table 2.2 Examples of various salts employed in PEs	8
Table 2.3 Solid fillers utilized in CPE systems	14
Table 2.4 Potential applications of PE	16
Table 2.5 Various type of iron oxides	19
Table 2.6 Applications of magnetite	21
Table 2.7 The integral $g(a)$ and differential $f(a)$ conversion function for most common mechanisms	25
Table 3.1 Preparation parameters of LiX-ENR-50 PEs	40
Table 3.2 Preparation parameters of MI-ENR-50 PEs	41
Table 3.3 Preparation parameters of Fe_3O_4 /ENR-50 composites	42
Table 3.4 Preparation parameters of LiX- Fe_3O_4 /ENR-50 CPEs	43
Table 4.1 T_g for various compositions of PE of LiX-ENR-50 where X = $COOCF_3^-$, I^- , $CF_3SO_3^-$, ClO_4^- and BF_4^-	60
Table 4.2 T_{onset} , $T_{0.5}$ and T_{max} for ENR-50 and the various LiX-ENR-50 with 10 wt% lithium salt and the lattice energy for the respective LiX	65
Table 4.3 The value of circuit components for various LiX-ENR-50 with 10 wt% lithium salt	70
Table 4.4 Glass transition temperature (T_g) for various MI-ENR-50 PEs	71
Table 4.5 The value of circuit components for various MI-ENR-50 with 10 wt% MI salt	82
Table 5.1 E_d and r values for purified ENR-50 calculated by FWO method	90
Table 5.2 Activation energy (E_d) in $kJ\ mol^{-1}$ and linear regression (r) of purified ENR-50 obtained by CR method at various heating rates	92
Table 5.3 E_d ($kJ\ mol^{-1}$) and r values for purified ENR-50 and LiX-ENR-50 PEs calculated by isoconversional methods	95
Table 5.4 Mean activation energy (E_d) in $kJ\ mol^{-1}$ and linear regression (r) of various LiX-ENR-50 PEs and purified ENR-50 obtained by CR method	98

Table 5.5	E_d (kJ mol ⁻¹) and r values for MI-ENR-50 PEs calculated by isoconversional methods	104
Table 5.6	Mean activation energy (E_d) in kJ mol ⁻¹ and linear regression (r) of various MI-ENR-50 PEs obtained by CR method	107
Table 6.1	FTIR peak positions and assignments for ENR-50, typical Fe ₃ O ₄ /ENR-50 nanocomposite, Fe ₃ O ₄ and ENR-50 reacted with KOH	117
Table 6.2	The T_g , exponent (n), pre-exponential factor (A) and linear regression (r) values for ENR-50 and the various Fe ₃ O ₄ /ENR-50 nanocomposites	123
Table 6.3	The value of circuit components for Fe₃O₄/ENR nanocomposites	131
Table 7.1	FTIR peak positions and assignments for ENR-50, Fe ₃ O ₄ /ENR-50 base composite and the 10 wt% LiX-Fe ₃ O ₄ /ENR-50 CPEs	139
Table 7.2	Glass transition temperature (T_g) for various compositions of LiX-Fe ₃ O ₄ /ENR-50 CPEs where X = COOCF ₃ ⁻ , I ⁻ , CF ₃ SO ₃ ⁻ , ClO ₄ ⁻ and BF ₄ ⁻	146
Table 7.3	T_{onset} , $T_{0.5}$ and T_{max} for neat ENR-50, Fe ₃ O ₄ /ENR-50 base composite and the various LiX-Fe ₃ O ₄ /ENR-50 containing 10 wt% lithium salt	150
Table 7.4	The value of circuit components for various LiX-Fe₃O₄/ENR-50 containing 10 wt% lithium salt	155
Table 8.1	E_d and r values for ENR-50 incorporated with 3.9 wt% Fe ₃ O ₄ particles (base composite) calculated by FWO and Kissinger methods	162
Table 8.2	Activation energy, E_d and linear regression (r) of Fe ₃ O ₄ /ENR-50 base composite obtained by CR method	164
Table 8.3	E_d and r values for LiX-Fe ₃ O ₄ /ENR-50 CPEs calculated by isoconversional methods	169
Table 8.4	Activation energy (E_d) in kJ mol ⁻¹ and linear regression (r) of various LiX-Fe ₃ O ₄ /ENR-50 CPEs obtained by CR method	170

LIST OF FIGURES

		Page
Figure 2.1	Various polymer host architectures for PE applications	11
Figure 2.2	Epoxidation of natural rubber (NR)	16
Figure 2.3	(a) Fe ₃ O ₄ coated- and (b) Fe ₃ O ₄ incorporated polymer composites	20
Figure 3.1	Home-made cell design for EIS testing	46
Figure 4.1	SEM micrographs of (a) purified ENR-50 and the PE of 10 wt% LiX incorporated ENR-50 where X = (b) COOCF ₃ ⁻ , (c) I ⁻ , (d) CF ₃ SO ₃ ⁻ , (e) ClO ₄ ⁻ , (f) BF ₄ ⁻	52
Figure 4.2	SEM and X-mapping micrographs (magnification 500x) for 10 wt% LiX-ENR-50 PEs where X = (a) COOCF ₃ ⁻ , (b) I ⁻ , (c) CF ₃ SO ₃ ⁻ , (d) ClO ₄ ⁻ , (e) BF ₄ ⁻	53
Figure 4.3	Typical FTIR spectra for (a) purified ENR-50 and the PEs of 10 wt% LiX-ENR-50 where X = (b) COOCF ₃ ⁻ , (c) I ⁻ , (d) CF ₃ SO ₃ ⁻ , (e) ClO ₄ ⁻ , (f) BF ₄ ⁻	55
Figure 4.4	Representative DSC thermograms for LiX-ENR-50 PEs containing 10 wt% LiX where X = (a) COOCF ₃ ⁻ , (b) CF ₃ SO ₃ ⁻ , (c) I ⁻ , (d) BF ₄ ⁻ and (e) ClO ₄ ⁻ [Arrow illustrates the T _g]	60
Figure 4.5	DSC thermograms of LiClO ₄ -ENR-50 PEs containing (a) 5, (b) 10, (c) 15, (d) 20, (e) 25 wt% of LiClO ₄ and (f) pristine LiClO ₄ [Arrow illustrates the T _g]	62
Figure 4.6	The (a) TG and (b) DTG curves for purified ENR-50 and various LiX-ENR-50 with 10 wt% lithium salt	64
Figure 4.7	Conductivity of various LiX-ENR-50 polymer electrolytes at 25 °C as a function of salt concentrations. (legend: x CF ₃ SO ₃ ⁻ , y I ⁻ , z COOCF ₃ ⁻ , * BF ₄ ⁻ , + ClO ₄ ⁻)	66
Figure 4.8	Nyquist plots for various LiX-ENR-50 with 10 wt% lithium salt where X = (a) COOCF ₃ ⁻ , (b) I ⁻ , (c) CF ₃ SO ₃ ⁻ , (d) ClO ₄ ⁻ and (e) BF ₄ ⁻ and (f) the equivalent circuit [red square = experimental data, green square = fitted data]	69
Figure 4.9	Typical FTIR spectra for (a) purified ENR-50 and the PE of 10 wt% MI incorporated ENR-50 where M = (b) Li ⁺ , (c) Na ⁺ , (d) K ⁺ and (e) Ag ⁺	73
Figure 4.10	SEM micrographs for ENR-50 incorporated with 10 wt% MI where M = (a) Li ⁺ , (b) Na ⁺ , (c) K ⁺ and (d) Ag ⁺	74
Figure 4.11	Element mapping micrographs for ENR-50 incorporated with 10 wt% MI where M = (a) Li ⁺ , (b) Na ⁺ , (c) K ⁺ and (d) Ag ⁺	76

Figure 4.12	(a) TG and (b) DTG curves for purified ENR-50 and ENR-50 incorporated with 10 wt% MI where M = Li ⁺ , Na ⁺ , K ⁺ or Ag ⁺ at a heating rate of 20 °C min ⁻¹	78
Figure 4.13	Variation of T _{onset} with different MI concentrations	79
Figure 4.14	Nyquist plot and the equivalent circuit for ENR-50 incorporated with 10 wt% MI where M = (a) Li ⁺ , (b) Na ⁺ , (c) K ⁺ and (d) Ag ⁺ [red square = experimental data, green square = fitted data]	81
Figure 5.1	(a) a-T plots and (b) (da/dT) derivative curves for purified ENR-50 at various heating rates [(i) 2, (ii) 10, (iii) 20, (iv) 30 and (v) 40 °C min ⁻¹]	88
Figure 5.2	Kissinger plot for purified ENR-50	89
Figure 5.3	FWO plots for purified ENR-50 at different a	89
Figure 5.4	Master plot of theoretical Z(a) against a for various reaction models and experimental data of purified ENR-50	91
Figure 5.5	(a) a-T plots and (b) (da/dT) derivative curves for LiX-ENR-50 PEs at a heating rate of 10 °C min ⁻¹ [X = CF ₃ SO ₃ ⁻ (blue), COOCF ₃ ⁻ (purple), I ⁻ (green), ClO ₄ ⁻ (black) and BF ₄ ⁻ (brown)]	94
Figure 5.6	Dependence of E _d values on a based on FWO method	96
Figure 5.7	Master plot of theoretical Z(a) against a for the various reaction models and experimental data of the PEs of LiX-ENR-50 where X= (a) COOCF ₃ ⁻ , (b) CF ₃ SO ₃ ⁻ , (c) I ⁻ , (d) BF ₄ ⁻ , (e-f) ClO ₄ ⁻ (first and second step) at a heating rate of 10 °C min ⁻¹	99
Figure 5.8	(a) a-T plots and (b) its (da/dT) derivative curves for MI-ENR-50 PEs at a heating rate of 10 °C min ⁻¹ [M = Li ⁺ (purple), Na ⁺ (red), K ⁺ (blue) and Ag ⁺ (black)]	103
Figure 5.9	Dependence of E _d values on a based on FWO method	105
Figure 5.10	Master plot of theoretical Z(a) against a for the various reaction models and experimental data of the PEs of MI-ENR-50 where M = (a) Li ⁺ (b) Na ⁺ , (c) K ⁺ and (d) Ag ⁺ at a heating rate of 10 °C min ⁻¹	108
Figure 6.1	Typical XRD pattern of Fe ₃ O ₄ /ENR-50 nanocomposite and the corresponding reference peak profile (JCPDS file no 19-629)	114
Figure 6.2	Typical FTIR spectra of (a) ENR-50, (b) Fe ₃ O ₄ /ENR-50 nanocomposite, (c) pristine Fe ₃ O ₄ and (d) ENR-50 reacted with KOH	115

Figure 6.3	SEM micrographs (350x magnification) of (a) ENR-50 and the ENR-50/Fe ₃ O ₄ composites containing (b) 2.8 wt% and (c) 9.4 wt% Fe ₃ O ₄ and the TEM micrographs of (d) Fe ₃ O ₄ particles and the ENR-50/Fe ₃ O ₄ composites containing (e) 2.8 wt% and (f) 9.4 wt% Fe ₃ O ₄	118
Figure 6.4	SEM and X-mapping micrographs of ENR-50 composited with 5.1 wt % Fe ₃ O ₄ showing the (a) surface at (i) low (100x) and (ii) high magnification (2500x) and (b) low magnification (100x) cross sectional profiles	119
Figure 6.5	The (a) TG and (b) DTG curves of (i) purified ENR-50 (green) and ENR-50 composited with (ii) 2.8 wt% (red), (iii) 3.9 wt% (brown), (iv) 5.1 wt% (purple), (v) 9.4 wt% (blue) and (vi) 16.3 wt% (orange) of Fe ₃ O ₄ (heating rate of 10 °C min ⁻¹)	125
Figure 6.6	Plot of AC conductivity versus angular frequency for ENR-50 and Fe ₃ O ₄ /ENR-50 nanocomposites with various wt% of Fe ₃ O ₄	127
Figure 6.7	The plot of s _{DC} conductivity against the wt% of Fe ₃ O ₄ in the composites	128
Figure 6.8	Nyquist plot for Fe ₃ O ₄ /ENR-50 nanocomposites containing (a) 2.8 wt%, (b) 3.9 wt%, (c) 5.1 wt%, (d) 9.4 wt%, (e) 16.3 wt% Fe ₃ O ₄ and (f) the equivalent circuit	130
Figure 7.1	Typical FTIR spectra for (a) pristine ENR-50, (b) Fe ₃ O ₄ /ENR-50 base composite and 10 wt% LiX-Fe ₃ O ₄ /ENR-50 CPEs where X = (c) COOCF ₃ ⁻ , (d) I ⁻ , (e) CF ₃ SO ₃ ⁻ , (f) ClO ₄ ⁻ and (g) BF ₄ ⁻	138
Figure 7.2	SEM micrographs of (a) Fe ₃ O ₄ /ENR-50 composite and CPE incorporated with 10 wt% LiX where X = (b) COOCF ₃ ⁻ , (c) I ⁻ , (d) CF ₃ SO ₃ ⁻ , (e) ClO ₄ ⁻ and (f) BF ₄ ⁻	141
Figure 7.3	SEM micrographs and X-mapping micrographs for 10 wt% LiX-Fe ₃ O ₄ /ENR-50 CPEs where X = (a) COOCF ₃ ⁻ , (b) I ⁻ , (c) CF ₃ SO ₃ ⁻ , (d) ClO ₄ ⁻ and (e) BF ₄ ⁻	142
Figure 7.4	TEM micrographs of (a) Fe ₃ O ₄ /ENR-50 composite and the 10 wt% LiX-Fe ₃ O ₄ /ENR-50 CPEs where X = (b) COOCF ₃ ⁻ , (c) ClO ₄ ⁻ , (d) CF ₃ SO ₃ ⁻ , (e) I ⁻ , (f) BF ₄ ⁻	144
Figure 7.5	The (a) TG and (b) DTG curves for (i) ENR-50 (orange), (ii) Fe ₃ O ₄ /ENR-50 base composite (light blue) and LiX-Fe ₃ O ₄ /ENR-50 CPEs where X = (iii) CF ₃ SO ₃ ⁻ (brown), (iv) BF ₄ ⁻ (red), (v) I ⁻ (purple), (vi) COOCF ₃ ⁻ (blue) and (vii) ClO ₄ ⁻ (green)	148
Figure 7.6	Conductivity for LiX-Fe ₃ O ₄ /ENR-50 CPEs as a function of salt concentrations at 25 °C	153

Figure 7.7	Nyquist plots for various LiX-Fe ₃ O ₄ /ENR-50 with 10 wt% lithium salt where X = (a) COOCF ₃ ⁻ , (b) I ⁻ , (c) CF ₃ SO ₃ ⁻ , (d) ClO ₄ ⁻ and (e) BF ₄ ⁻ and (f) the equivalent circuit [red square = experimental data, green square = fitted data]	154
Figure 7.8	Schematic diagram for the carrier movement in CPE	155
Figure 8.1	(a) a-T plots and (b) its (da/dT) derivative curves for ENR-50 incorporated with 3.9 wt% Fe ₃ O ₄ particles (base composite) at various heating rates [(i) 2, (ii) 10, (iii) 20, (iv) 30 and (v) 40 °C min ⁻¹]	160
Figure 8.2	Kissinger plot for ENR-50 incorporated with 3.9 wt% Fe ₃ O ₄ particles (base composite) [solid line = peak 1 and dashed line = peak 2]	161
Figure 8.3	FWO plots for ENR-50 incorporated with 3.9 wt% Fe ₃ O ₄ particles (base composite) at different a [solid line = peak 1 and dashed line = peak 2]	162
Figure 8.4	Master plot of theoretical Z(a) against a for various reaction models and experimental data of ENR-50 incorporated with 3.9 wt% Fe ₃ O ₄ particles (base composite) (a) peak 1 and (b) peak 2	165
Figure 8.5	(a) a-T plots and (b) (da/dT) derivative curves for LiX-Fe ₃ O ₄ /ENR-50 CPEs at a heating rate of 10 °C min ⁻¹ [X= CF ₃ SO ₃ ⁻ (blue), COOCF ₃ ⁻ (purple), I ⁻ (green), ClO ₄ ⁻ (black) and BF ₄ ⁻ (brown)]	167
Figure 8.6	Master plot of theoretical Z(a) against a for various reaction models and experimental data of the CPEs of LiX-Fe ₃ O ₄ /ENR-50 where X= (a) COOCF ₃ ⁻ , (b) CF ₃ SO ₃ ⁻ , (c) I ⁻ , (d) BF ₄ ⁻ , (e-f) ClO ₄ ⁻ (step 1 and 2) at a heating rate of 10 °C min ⁻¹	171

LIST OF SYMBOLS

a	Degree of conversion
b	Heating rate
s	Conductivity
m	Mobility
da/dt	Rate of conversion
$f(a)$	Function of conversion
$g(a)$	Integral function of conversion
A	Pre-exponential factor
E	Activation energy
E_d	Degradation activation energy
K	Rate constant
N	Number of charge carrier
Q	Constant phase element
R	Gas constant
T	Absolute temperature
T_g	glass transition temperature
$T_{0.5}$	Temperature at 50% degradation
T_{onset}	Onset of decomposition temperature
T_{max}	Temperature at maximum decomposition rate
T_p	Temperature for maximum degradation rate
Z_w	Warburg element

LIST OF ABBREVIATIONS

AAS	Atomic absorption spectroscopy
BL	γ -butyrolactone
CPE	Composite polymer electrolyte
CR	Coats and Redfern
DBP	Dibutyl phthalate
DEC	Diethyl carbonate
DMC	Dimethyl carbonate
DMF	Dimethyl formamide
DOA	Dioctyl adipate
DOP	Dioctyl phthalate
DSC	Differential scanning calorimetry
DSSC	Dye-sensitized Solar Cell
EC	Ethylene carbonate
ECA	Electrical conductive adhesive
((EG) ₄ DVE)	Oligo(ethylene glycol) ₄ divinyl ether
EIA	Energy Information Administration
EIS	Electrochemical impedance spectroscopy
EMI	Electromagnetic interference
ENR-50	Epoxidized natural rubber
FTIR	Fourier transform infrared
FTO	Fluorine-doped tin oxide
FWO	Flynn-Wall-Ozawa
GPE	Gel polymer electrolyte
GS	Glycol sulphide
MAN	Maleic anhydride

MEC	Methyl ethyl carbonate
MMT	Montmorillonite
MRI	Magnetic resonance imaging
MSAC	Modified silica-aluminium-carbon
NR	Natural rubber
NBR	Nitrile rubber
PANI	Polyaniline
PC	Propylene carbonate
PDLLA	Poly(D,L-lactide)
PE	Polymer electrolyte
PEMA	Poly(ethyl methacrylate)
PEO	Poly(ethylene oxide)
PHB	Poly(3-hydroxybutyrate)
PHBV	Poly(3-hydroxybutyrate-co-3-hydroxyvalerate)
PLGA	Poly(lactic-co-glycolic acid)
PMMA	Poly(methyl methacrylate)
PPy	Polypyrrole
PU	Polyurethane
PVA	Poly(vinyl alcohol)
PVC	Poly(vinylchloride)
PVdF	Poly(vinylidene fluoride)
PVP	Poly(N-vinyl pyrrolidone)
SBR	Styrene butadiene rubber
SEM	Scanning electron microscopy
SPEEK	Sulphonated polyether ether ketone
SWCNT	Single wall carbon nanotube
TEM	Transmission electron microscopy

TG	Thermogravimetric
TGME	Tetraethyleneglycol dimethylether
TIM	Thermal interface material
UV	Ultra-violet
XRD	X-ray diffraction

SIFAT TERMA DAN KEKONDUKSIAN ION BAGI KOMPOSIT BERASASKAN ENR-50 POLIMER ELEKTROLIT

ABSTRAK

Sintesis polimer elektrolit (PE) dan komposit polimer elektrolit (CPE) menggunakan getah asli terepoksida (ENR-50) sebagai matrik perumah dan nanozarah magnetit (Fe_3O_4) sebagai pengisi tak organik telah dijalankan. Ini dicirikan oleh FTIR, SEM/**pemetaan-X**, TEM, XRD, DSC, TGA dan EIS. Pengaruh garam litium, LiX (**yang mana** $X = \text{BF}_4^-$, I^- , CF_3SO_3^- , COOCF_3^- and ClO_4^-) dengan pelbagai anion dan garam iodida, MI (**yang mana** $M = \text{Li}^+$, Na^+ , K^+ and Ag^+) dengan kation berbeza terhadap sifat-sifat dan degradasi PE disiasat. Ini diikuti oleh kajian kehadiran serentak nanozarah Fe_3O_4 dalam pelbagai sistem LiX-ENR-50 PE. Kajian mengenai komposit $\text{Fe}_3\text{O}_4/\text{ENR-50}$ seadanya juga dilakukan sebagai perbandingan. **Kecenderungan** kestabilan terma dan kekonduksian ionik untuk LiX-ENR-50 PE **megikut tertib** $\text{LiBF}_4 \gg \text{LiCF}_3\text{SO}_3 \sim \text{LiCOOCF}_3 > \text{LiI} \gg \text{LiClO}_4$. LiClO_4 sukar diceraikan dan membentuk agregat LiClO_4 dalam matrik ENR-50 menghasilkan PE dengan kestabilan terma rendah dan kekonduksian ionik rendah. LiCF_3SO_3 , LiCOOCF_3 dan LiI memberikan interaksi sederhana dengan ENR-50 dan PE masing-masing mempamerkan kekonduksian ionik dan ciri-ciri terma yang sederhana. Pembukaan gelang epoksida dan pengkompleksan atau tindak balas penyambung-silang di dalam dan di antara rangkaian ENR-50 yang melibatkan ion BF_4^- telah menghasilkan $\text{LiBF}_4\text{-ENR-50}$ PE dengan kestabilan terma dan kekonduksian ionik unggul berbanding dengan LiX-ENR-50 PE lain dalam kajian ini. Ciri-ciri impedan MI-ENR-50 PE berkait rapat dengan keterlarutan, interaksi dan morfologi garam MI di dalam ENR-50. Keterlarutan garam MI di dalam ENR-50 mengikut tren menurun $\text{LiI} > \text{NaI} > \text{KI} > \text{AgI}$. Dalam PE, kebanyakan LiI wujud dalam ion dan Li^+ pseudo-silang dengan epoksida di dalam rangkaian ENR-50. Garam MI lain sukar diceraikan dan mempamerkan interaksi lemah atau tiada dengan ENR-50. Kestabilan terma ENR-50 dalam PE bergantung kepada jenis logam garam MI. Logam alkali seperti Li, Na dan K tidak banyak mempengaruhi kestabilan ENR-50. Walau bagaimanapun, kehadiran AgI menyahstabilkan ENR-50 di dalam PE. Degradasi ENR-50 dalam LiClO_4^- , NaI - dan KI -ENR-50 PE adalah serupa dengan ENR-50 tulen disebabkan oleh interaksi garam-ENR-50 yang lemah. Ia dimulakan dengan tindak balas tertib pertama (F_1) diikuti oleh reaksi penyebaran kawalan 3-dimensi (D_3). Kehadiran garam lain dalam PE menyebabkan degradasi ENR-50 mengikut hanya model D_3 . Pseudo-silang atau pengkompleksan antara LiX dan ENR-50 menghasilkan struktur padat yang menghadkan produk degradasi

terlepas dari sistem. Bagi AgI-ENR-50, sekatan adalah disebabkan oleh berat molekul zarah AgI yang tinggi dalam sistem. Dalam komposit $\text{Fe}_3\text{O}_4/\text{ENR-50}$, matrik ENR-50 memberikan kawalan pada zarah Fe_3O_4 dengan saiz <20 nm. Zarah Fe_3O_4 juga mempengaruhi sifat-sifat elektrik komposit. Kekonduksian elektrik komposit meningkat dengan peningkatan kandungan Fe_3O_4 dalam komposit. Penambahan zarah Fe_3O_4 menyahstabilkan ENR-50 dalam komposit. Pada kandungan Fe_3O_4 yang rendah dalam komposit, zarah menggalakkan degradasi awal ENR-50. Walau bagaimanapun, keberkesanan pemangkin zarah Fe_3O_4 pada kandungan tinggi telah dikurangkan disebabkan oleh aglomerasi zarah. $\text{LiX-Fe}_3\text{O}_4/\text{ENR-50}$ CPE iaitu $\text{X} = \text{COOCF}_3^-$, CF_3SO_3^- , I^- dan ClO_4^- , menunjukkan kelakuan terma yang serupa dengan LiX-ENR-50 PE masing-masing. Walau bagaimanapun, $\text{LiBF}_4\text{-Fe}_3\text{O}_4/\text{ENR-50}$ adalah kurang stabil berbanding dengan $\text{LiBF}_4\text{-ENR-50}$ PE. Dengan pengecualian $\text{LiBF}_4\text{-Fe}_3\text{O}_4/\text{ENR-50}$, kekonduksian CPE ditingkatkan sebanyak 1-2 kaliganda berbanding LiX-ENR-50 PE masing-masing. Kehadiran zarah Fe_3O_4 telah memudahkan pergerakan pembawa cas melalui penciptaan cas ruang pada antara muka zarah/polimer serta peningkatan amorfus matrik ENR-50. Walau bagaimanapun, $\text{LiBF}_4\text{-Fe}_3\text{O}_4/\text{ENR-50}$ memberikan kekonduksian lebih rendah berbanding dengan $\text{LiBF}_4\text{-ENR-50}$ kerana penceraian Li^+BF_4^- yang lemah disebabkan oleh zarah Fe_3O_4 . Berbeza dengan ENR-50 tulen, kehadiran zarah Fe_3O_4 dalam komposit $\text{Fe}_3\text{O}_4/\text{ENR-50}$ mengubah degradasi awal ENR-50 kepada model A_2 . Mereka bertindak sebagai nukleus yang menyebarkan haba kepada rangkaian ENR-50 sekitarnya dan memulakan degradasi ENR-50. Sebaliknya, degradasi keseluruhan ENR-50 dalam $\text{LiX-Fe}_3\text{O}_4/\text{ENR-50}$ CPE adalah hanya dikawal oleh penyebaran kerana kelikatan tinggi pada sistem.

THERMAL BEHAVIORS AND IONIC CONDUCTIVITY OF COMPOSITE ENR-50-BASED POLYMER ELECTROLYTES

ABSTRACT

The synthesis of polymer electrolytes (PEs) and composite polymer electrolytes (CPEs) using epoxidized natural rubber (ENR-50) as the host matrix and magnetite (Fe_3O_4) nanoparticles as the inorganic filler was carried out. These were characterized by FTIR, SEM/X-mapping, TEM, XRD, DSC, TGA and EIS. The influence of lithium salt, LiX (where $X = \text{BF}_4^-$, I^- , CF_3SO_3^- , COOCF_3^- and ClO_4^-) with various anions and iodide salt, MI (where $M = \text{Li}^+$, Na^+ , K^+ and Ag^+) with different cations on the properties and degradation of PEs was investigated. This was followed by the study of the simultaneous presence of Fe_3O_4 nanoparticles in various LiX-ENR-50 PE systems. The study on sole Fe_3O_4 /ENR-50 composites was also performed for comparison purposes. The trend in thermal stability and ionic conductivity of LiX-ENR-50 PEs is in the order of $\text{LiBF}_4 \gg \text{LiCF}_3\text{SO}_3 \sim \text{LiCOOCF}_3 > \text{LiI} \gg \text{LiClO}_4$. The LiClO_4 hardly dissociates and formed LiClO_4 aggregates within the ENR-50 matrix that resulted in a PE with low thermal stability and low ionic conductivity. The LiCF_3SO_3 , LiCOOCF_3 and LiI exert moderate interactions with the ENR-50 and their respective PEs exhibit moderate ionic conductivity and thermal property. The occurrence of epoxide ring opening and complexation or cross-linking reactions in and between the ENR-50 chains that involve BF_4^- ions have produced a LiBF_4 -ENR-50 PE with superior thermal stability and ionic conductivity as compared to other LiX-ENR-50 PEs studied in this work. The impedance properties of MI-ENR-50 PEs are closely related to the solubility, interaction and the outcome morphology of MI salt in the ENR-50. The solubility of MI salt in the ENR-50 follows the decreasing trend of $\text{LiI} > \text{NaI} > \text{KI} > \text{AgI}$. In PEs, the LiI mostly exists in ions and the Li^+ are pseudo-crosslinked with the epoxide in the ENR-50 chains. Other MI salts are hardly dissociated in the ENR-50 which exert weak or no chemical interaction with the ENR-50. The thermal stability of ENR-50 in PEs is dependant on the type of metal in the MI salt. The alkali metal like Li, Na and K does not greatly influence the stability of ENR-50. Nonetheless, the presence of AgI destabilizes the ENR-50 in PE. The degradation of ENR-50 in LiClO_4^- , NaI - and KI -ENR-50 PE is similar to purified ENR-50 due to weak salt-ENR-50 interaction. It initiates with first-order reaction (F_1) followed by 3-dimensional diffusion control (D_3) reaction. The presence of other salts in PE caused the degradation of ENR-50 to follow only a D_3 type model. The pseudo-crosslinking or complexation between the LiX and

ENR-50 produces a compact structure that restricts the degradation products to escape from the system. As for AgI-ENR-50, the restriction is mainly caused by the high molecular weight of AgI particles in the system. In $\text{Fe}_3\text{O}_4/\text{ENR-50}$ composites, the ENR-50 matrix exerts control on the Fe_3O_4 particles with a size of < 20 nm. The Fe_3O_4 particles also affect the electrical properties of the composites. The electrical conductivity of the composites increases with the increase in Fe_3O_4 loading in the composite. The addition of Fe_3O_4 particles thermally destabilized the ENR-50 in the composites. At low loading of Fe_3O_4 in the composite, the particles promote an early degradation of ENR-50. Nevertheless, the catalytic effectiveness of the Fe_3O_4 particle at higher loading was reduced due to particles agglomerations. $\text{LiX-Fe}_3\text{O}_4/\text{ENR-50}$ CPEs where $X = \text{COOCF}_3^-$, CF_3SO_3^- , I^- and ClO_4^- , demonstrate similar thermal behavior as their LiX-ENR-50 PE counterparts. However, the $\text{LiBF}_4\text{-Fe}_3\text{O}_4/\text{ENR-50}$ is thermally less stable as compared to the respective $\text{LiBF}_4\text{-ENR-50}$ PE. With the exception of $\text{LiBF}_4\text{-Fe}_3\text{O}_4/\text{ENR-50}$, an improvement of 1-2 orders of magnitude in CPEs' conductivity is observed as compared to the respective LiX-ENR-50 PE counterparts. The presence of Fe_3O_4 particles facilitated the movement of charge carrier via space-charge creation at the particle/polymer interface as well as the increment of amorphocity of the ENR-50 matrix. Nevertheless, the $\text{LiBF}_4\text{-Fe}_3\text{O}_4/\text{ENR-50}$ gave lower conductivity as compared to $\text{LiBF}_4\text{-ENR-50}$ due to poorer Li^+BF_4^- dissociation caused by Fe_3O_4 particles. In contrast to purified ENR-50, the presence of Fe_3O_4 particles in the $\text{Fe}_3\text{O}_4/\text{ENR-50}$ composite changed the initial degradation of ENR-50 to A_2 model. They act as nucleus that spread the heat to the surrounding ENR-50 chains and initiates the ENR-50 degradation. On the other hand, the whole degradation of ENR-50 in $\text{LiX-Fe}_3\text{O}_4/\text{ENR-50}$ CPEs is solely controlled by diffusion due to high viscosity of the system.

CHAPTER 1

INTRODUCTION

1.1 A brief overview

There has been an enormous increase in the global demand for energy supply due to industrial development and population growth nowadays. The report by U.S. Energy Information Administration (EIA) in 2009 has also predicted that the world's energy consumption will double (~30-40 TW) in 2030 [1]. Today, the main energy resources are dependent on fossil fuels (viz. oil, coal and natural gas) followed by nuclear. However, the recent unrest in Middle-East, carbon emission issues and Fukushima nuclear crisis have fueled the need for development of new types of electrical power generation and storage systems.

In 1978, Armand highlighted the potential applications of polymer electrolyte (PE) in energy generation and storage systems [2]. PE as solid state ionic conductors is one of the main components in batteries, supercapacitors, fuel cells or solar cells. Thus the research on PE is bound to play a critical role in meeting global energy challenge. Furthermore, the development of PE also benefits electronic industries as it brings revolution on device's architecture **and also** to the biomedical industries by implementation of high performance actuators and sensors.

1.2 Problem statements

Epoxidized natural rubber with 50% epoxidation (ENR-50) is a green polymer that commonly available in Malaysia. The use of ENR-50 ultimately reduces the environment impact of hazardous products as well as the dependency of petroleum-based synthetic polymers. Furthermore, the available of polar oxirane groups in the polymer chains imparts electron-donating

characteristic to ENR-50. It allows interaction with carrier ions like Li^+ thus provides an effective conduction path for carrier ions [3]. The amorphous nature, good elasticity and adhesion properties also give added values for ENR-50 to adopt as polymer host for PE application [4]. These characteristics allow ENR-50 to form flexible film, as well as provide good contact between the electrolyte and electrodes. The potential applications of ENR-50 PE lie in various fields such as battery or cell, capacitor, sensor and many more. Mohamed and co-workers [5] has previously demonstrated the application of ENR-50 PE in the lithium-air primary cells. The discharge characteristic and specific energy for the cell are reported.

Although the research on ENR-50 PE has started about a decade, the publication on ENR-50-based PE is relatively scarce. Thus far, most of the ENR-50-based PE studies concern only on the preparation of Li^+ -ENR-50 blends of ternary (without organic plasticizer) or quaternary (with organic plasticizer) systems. These studies mainly focused on the conductivity of PE as a function of Li salt concentration, organic plasticizer loading or polymer blend ratio. Therefore, there remain some loop-holes in the research of ENR-50-based PEs. These are;

- (a) There are scarcely any studies on the influence of various lithium salts to the performance of ENR-50 PEs [3].
- (b) The studies have been limited mostly to lithium salts [3-6].
- (c) Limited reports on inorganic fillers incorporated in ENR-50-based PE systems (ENR-based composite polymer electrolyte (CPE)) [6].
- (d) Very little information is available on the thermal properties, degradation kinetics and mechanisms of ENR-50-based PEs or the respective CPEs [3-6].

The research on (a) to (d) above is of fundamental and technological importance. The study on these systems inevitably contributes to the field of PE.

1.3 Research aim and objectives

Section 1.2 above reveals that there are some research areas in ENR-based PEs to be explored. Hence, the aim of this work is to investigate the electrical and thermal properties of some ENR-50-based PEs using single polymer system in which a variety of salts and filler is **to be** incorporated.

The objectives of this study **are**:

- (a) To synthesize and characterize a series of LiX- and MI-ENR-50 PEs (where $X = \text{COOCF}_3, \text{CF}_3\text{SO}_3, \text{I}, \text{ClO}_4, \text{BF}_4$ and $M = \text{Li}, \text{Na}, \text{K}, \text{Ag}$)
- (b) To study the influence of anions (X^-) of LiX and cations (M^+) of MI on the properties of ENR-50 PEs
- (c) To synthesize and characterize the LiX- Fe_3O_4 /ENR-50 composite polymer electrolytes (CPEs)
- (d) To **study** the role of Fe_3O_4 particles on the properties of ENR-50 CPEs
- (e) To conduct the degradation study on ENR-50-based PEs and CPEs above

1.4 Scope of study

This study has been limited to the synthesis of ENR-50-based polymer electrolytes (PEs). In binary systems, the effect of anions of LiX salts (**where $X = \text{CF}_3\text{SO}_3^-, \text{COOCF}_3^-, \text{I}^-, \text{BF}_4^-$ and ClO_4^-**) as well as cations of MI salts (**where $M = \text{Li}^+, \text{Na}^+, \text{K}^+$ and Ag^+**) on the property of ENR-50 PE was studied. In the case of ternary systems, the magnetite (Fe_3O_4) particles were incorporated into the LiX-ENR system. The influence of this filler to the structural, **ionic conductivity and thermal property** changes is investigated and compared to their binary PE systems.

Although the main intention of this research project is focused on ENR-50-based PEs and CPEs, nevertheless, the study on the sole $\text{Fe}_3\text{O}_4/\text{ENR-50}$ composites is also included in view of its technological potential besides for comparison purposes. Also of interest is the thermal degradation of ENR-50 in various PE, CPE or composite systems. It involves the determination of kinetic parameter and degradation mechanism by 4 known methods: Kissinger, Flynn-Wall-Ozawa (FWO), Coats-Redfern (CR) and Criado.

1.5 Thesis layout

This thesis consists of nine chapters. Chapter 1 gives an overview of the thesis which includes a brief overview and problem statements that lead to this research study, the scope and research objectives as well as the thesis layout. Chapter 2 provides a detail literature survey on the progress of the related topics while Chapter 3 describes the materials used as well as the preparation procedures and characterization techniques. Chapter 4 focuses on the preparation and characterization of binary salt-ENR-50 PE systems. The effect of anions of lithium salt (LiX) and the effect of cations of iodide salt (MI) on the impedance and thermal properties as well as thermal degradation kinetics of the ENR-50-based PEs is discussed. The degradation study of the various PEs are presented in Chapter 5. Chapter 6 presents the results and discussion for the $\text{Fe}_3\text{O}_4/\text{ENR-50}$ composites. It covers the synthesis, characterization, impedance and thermal studies. The following Chapter 7 focuses on the synthesis and characterization of $\text{LiX-Fe}_3\text{O}_4/\text{ENR-50}$ CPE systems. The role of the Fe_3O_4 particles in the systems of $\text{LiX-Fe}_3\text{O}_4/\text{ENR-50}$ with respect to the structural, physical, impedance and thermal properties is investigated. As for Chapter 8, it discusses the thermal degradation of the $\text{Fe}_3\text{O}_4/\text{ENR-50}$ composite as well as $\text{LiX-Fe}_3\text{O}_4/\text{ENR-50}$ CPE systems. Finally, the overall summary of the research findings and recommendation for future works is addressed in Chapter 9.

1.6 References

1. "2009 EIA report", [http:// www.eia.doe.gov/oiaf/ieo/index.html](http://www.eia.doe.gov/oiaf/ieo/index.html) [access date: 08/11/2012]
2. F.M. Gray, Solid polymer electrolytes: Fundamentals and technological applications, VCH Publishers Inc., New York, US, 1991
3. W. Klinklai, S. Kawahara, T. Mizumo, M. Yoshizawa, Y. Isono and H. Ohno, *Solid State Ionics*, 168, 131, 2004
4. R. Idris, M.D. Glasse, R.J. Latham, R.G. Linford and W.S. Schlindwein, *J. Power Sources*, 94, 206, 2001
5. S.N. Mohamed, N.A. Johari, A.M.M. Ali, M.K. Harun and M.Z.A. Yahya, *J. Power Sources*, 183, 351, 2008
6. S.A.M. Noor, A. Ahmad, I.A. Talib and M.Y.A. Rahman, *Ionics*, 17, 451, 2011

CHAPTER 2

LITERATURE REVIEW

2.1 Polymer electrolytes

Polymer electrolyte (PE) is a class of solid state ionic conductor. It can be prepared by dissolving certain inorganic salts into a suitable polymer. PE has the advantages over conventional liquid electrolytes in terms of being more flexible and stable, offers better processability, lighter, safer and alleviate leakage, evaporation of solvent or flammability [1, 2]. PE has been used as both separator and electrolyte in most of the applications. In order to function optimally, the PE must have sufficient ionic conductivity (ca. $\sim 10^{-3}$ - 10^{-2} Scm⁻¹) at room temperature, electrochemically, thermally and mechanically stable, compatible with electrode materials and readily available and inexpensive [3].

Many efforts have been resourced in order to diversify and to improve the performance and functionalities of current PEs. The modifications can be done via manipulating the compositions of PE including the types of salt, polymer host's structure, or addition of additives into the PE.

2.1.1 Salts

The choice of salt is one of the basic factors that tailor the performance of PE. The compatibility, dissolution and interaction between the salt and the polymer greatly influence the PE's performance outcome. In general, for higher conductivity of PEs, the ideal salt should be highly solvated, stable, inert, non-toxic and compatible [1].

Lithium salt perhaps is the most studied salt in PE applications. Lithium ion (Li⁺) with light mass, high energy and power density [1] is a suitable source of charge carrier in PEs. Numerous lithium salts have been studied in PE systems, from simple lithium salts such as lithium iodide (LiI) to polyanionic lithium salts like

poly(lithium sorbate). Table 2.1 summarizes some previously reported lithium salts in poly(ethylene oxide) (PEO)-based PE systems.

Table 2.1 Lithium salts in PEO-based PE systems.

Polymer host	Lithium salt	Reference
PEO	LiI, LiClO ₄ , LiCF ₃ SO ₃	[4]
	Li _{1.3} Al _{0.3} Ti _{1.7} (PO ₄) ₃	[5]
	Li ₂ SO ₄ , LiCF ₃ SO ₃	[6]
	Li(C ₈ F ₁₇ SO ₃)	[7]
	Li(CF ₃ SO ₂) ₂ N	[8]
	LiCl, LiClO ₄	[9]
	LiPF ₆	[10]
	LiN(SO ₂ CF ₂ CF ₃) ₂	[11]
	Poly(lithium sorbate), poly(lithium muconate)	[12]
	Lithium 4,5-dicyano-2-(trifluoroalkyl)imidazole,	[13]
	lithium 4,5-dicyano-2-(pentafluoroalkyl)imidazole	
	Lithium bis(oxalate)borate	[14]
	poly(2-oxo-1-difluoroethylene sulfonylimide)	[15]
	lithium borate, lithium aluminate	[16]

Inorganic salt other than lithium have also been investigated. Monovalent cation salts like sodium tetrafluoroborate (NaBF₄) and potassium tetrafluoroborate (KBF₄) [17], divalent cation salts like magnesium perchlorate (Mg(ClO₄)₂) [18] and copper (II) triflate (Cu(CF₃SO₃)₂) [19], and mixed cations salt such as Zn_{1-x}Cu_x(CF₃SO₃)₂ [20] are some examples. Further lists are given in Table 2.2. The performance of some of these cations has been proven to be as effective as or even better than Li⁺ counterparts. For instance, Rietman et al. [17] have prepared complex of PEO with alkali metal salts, MBF₄ and MCF₃SO₃ (where M = Li, Na, K, Rb or Cs). The ionic conductivity in the series of MBF₄/PEO PEs and MCF₃SO₃/PEO PEs follows the order of cations; Na⁺ >> Li⁺ > K⁺, Cs⁺ >> Rb⁺ and Cs⁺, Rb⁺ > K⁺, Na⁺ >> Li⁺ respectively. The results show that the trend of ionic conductivity in the PEs is determined by the synergy of cation and anion of the salts used in the polymer host.

Besides single salt PE systems, some mixed salt systems have also been reported including those systems with different anions, i.e. lithium borate mixed

with lithium aluminate in PEO [21] and with different cations i.e. NaI and AgI in PEO [22] and PVA [23] and so on. According to the reports, mixed salt systems display higher ionic conductivity than the corresponding single salt PEs.

Table 2.2: Examples of various salts employed in PEs.

Metal/cation	Example of salts	Reference
Sodium	NaCF ₃ SO ₃ , NaBF ₄	[17]
	NaI	[22-23]
	NaSCN	[24]
	NaIO ₄	[25]
	NaBr	[26]
	NaClO ₄	[27]
	NaPO ₃	[28]
	NaF	[29]
	NaClO ₃	[30]
	NaBiF ₄	[31]
Potassium	KCF ₃ SO ₃ , KBF ₄	[17]
	KI	[32]
	KNO ₃	[33]
	KBrO ₃	[34]
	KOH	[35]
Silver	AgCF ₃ SO ₃	[36]
	AgNO ₃	[37]
	AgI, AgBr, AgCl	[38]
Magnesium	Mg(ClO ₄) ₂	[18]
	Mg(NO ₃) ₂	[39]
	MgN(CF ₃ SO ₂) ₂	[40]
	MgI ₂	[41]
Copper	Cu(CF ₃ SO ₃) ₂	[19]
Zinc/copper	Zn _{1-x} Cu _x (CF ₃ SO ₃) ₂	[20]
Rubidium	RbCF ₃ SO ₃ , RbBF ₄	[17]
Cesium	CsCF ₃ SO ₃ , CsBF ₄	[17]
Barium	BaN(CF ₃ SO ₂) ₂	[40]
Calcium	CaN(CF ₃ SO ₂) ₂	[40]
Strontium	SrN(CF ₃ SO ₂) ₂	[40]
Ammonium	NH ₄ CF ₃ SO ₃	[42]
	NH ₄ NO ₃	[43]
	NH ₄ HSO ₄	[44]
	NH ₄ I	[45]
	NH ₄ F	[46]

2.1.2 Polymer hosts

The main criterion of a polymer host with respect to PE applications is the ability of salt solvation. Thus, the polymers containing polar groups like

polyethers, polyesters, polyimides and polythiols are the focus of most researchers. Thermoplastic polymer hosts like poly(ethylene oxide) (PEO) [4, 6, 8, 10], poly(vinylchloride) (PVC) [25], poly(vinyl alcohol) (PVA) [26], elastomer rubber polymer hosts like nitrile rubber (NBR) [47, 48] and epoxidized natural rubber [49, 50] are some of the examples. Recently, in view of the environment issue faced today, the use of green polymers such as chitosan [42, 43], cellulose acetate [51], potato starch [52] have received attention.

Besides the homopolymers mentioned above, polymer host based on copolymers are also found in literature. These are block copolymers, i.e. polyacrylonitrile-*b*-polyethylene glycol [53], comb-like or grafted copolymers, i.e. polyimide/poly(ethylene glycol) methyl ether methacrylate [54] and alternating copolymers, i.e. maleic anhydride (MAN) and oligo(tetra-ethylene glycol)divinyl ether ((EG)₄DVE) [55]. Introducing of copolymeric unit in the main polymer structure reduces the crystallinity and increase the flexibility of the main polymer chains [56]. Hence the copolymers may exhibit better ionic conductivity as compared to their homo analogue.

In some of the cases, the polymer host is cross-linked to obtain better mechanical, thermal, chemical and dimensional stability. This can be done via physical methods using ultra-violet (UV) curing [57], gamma irradiation [58] or chemically cross-linked the polymer with suitable cross-linking agents [59-61]. In general, cross-linking reaction produces a polymer host with three-dimensional (3-D) networks that is more resistant to mechanical, thermal or dimensional changes.

Blending second polymer component with primary polymer host is an alternative way to improve the host's properties and functionalities. The mechanical strength [62, 63], adhesiveness [64], ionic conductivity [28] of the blend maybe improve via the addition of a second polymer component. Bhide and Hariharan [28] reported that the NaPO₃-PEO/PEG400 system exhibited an enhancement in the ionic conductivity of about two orders of magnitude as

compared to the NaPO₃-PEO system. The improvement of ionic conductivity in the blend system is due to the increment of amorphous phase in PEO that facilitates the charges' transportations. Nevertheless, the effectiveness or the performance of a blend system depends on various factors like the ratio of the polymers, mutual interactions between all the components in the system, preparation method etc. For instance, in the system of Li⁺-poly (vinylidene fluoride)-poly(ethyl methacrylate) (PVdF/PEMA), the ionic conductivity is enhanced at low wt% of PEMA, whereas it decreases at higher wt% due to the increment in crystallinity domains by PEMA in the system [65]. Figure 2.1 summarizes various polymer host architectures in PE applications.




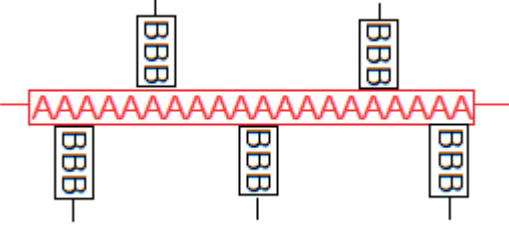

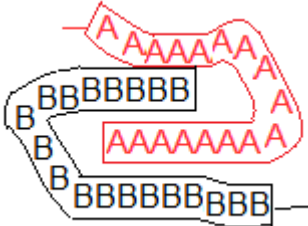
Types		Structure
(a) homopolymer		
(b) copolymer	Alternating	
	Block	
	Grafted	
(c) cross-linked polymer		
(d) polymer blend		

Figure 2.1: Various polymer host architectures for PE applications.

2.1.3 Additives

2.1.3.1 Organic plasticizers

Organic plasticizers are generally referred to as organic compounds with low molecular weight and high dielectric constants (polar). The main role of this small compound is to solvate the salt, increase the mobility or flexibility of the host polymer chains, and reduce ion pairing of salt which in turn improves the ionic conductivity of a PE [3, 56]. Due to their salts' solvation ability, they are also term as "polar solvent" and the resulting PE is categorized as gel polymer electrolyte (GPE). The most commonly used organic plasticizers are perhaps ethylene carbonate (EC) and propylene carbonate (PC). Intensive studies of GPE systems based on these plasticizers can be found in literature *viz.* Li⁺/EC+PC/ENR [49, 50], NH₄⁺/EC/PVA-chitosan [66], Li⁺/EC/PMMA [67], Li⁺/PC/PVAc-PMMA [68]. Other organic plasticizers are dimethyl carbonate (DMC), diethyl carbonate (DEC), dimethyl formamide (DMF), methyl ethyl carbonate (MEC), glycol sulphide (GS), g-butyrolactone (BL) [69] tetraethyleneglycol dimethylether (TGME) [70, 71], tetraglyme [72], dibutyl phthalate (DBP) [73, 74], dioctyl adipate (DOA) and dioctyl phthalate (DOP) [25]. **In general, increasing the organic plasticizer content in a PE ultimately enhances the ionic conductivity. Nonetheless, this is usually accompanied with a decrement in mechanical properties and a reduction in the system's compatibility.**

2.1.3.2 Fillers

Another popular approach to improve the property of PEs is by dispersing solid fillers in a PE system. This type of system is known as composite polymer electrolyte (CPE). In the early 80's, a pioneering work incorporating inert ceramic filler of α -alumina (α -Al₂O₃) into the Li⁺/PEO system was carried out by Weston and Steele [75]. They found that an additional of 10 vol% α -Al₂O₃ fillers greatly

improved the mechanical strength of the CPE but the ionic conductivity is barely affected. Later on, CPE researches extended to different phases of alumina like β - Al_2O_3 and γ - Al_2O_3 , and others ceramic fillers like silica (SiO_2) and zeolite $[(\text{Al}_2\text{O}_3)_{12}(\text{SiO}_2)_{12}]$. These inert fillers not only provide the mechanical strength to the system but also enhance the CPE's ionic conductivity. It is generally accepted that the enhancement of ionic conductivity of a ceramic-added PE is through the filler's percolation and increment of the polymer's amorphicity in the system. As fillers are connected into paths according to percolation theory, there are more conduction routes for ions transportation. Besides, the presence of fillers also prevent the recrystallization of polymer, hence the polymer chains are more flexible and able to assist the migration of ions. Nevertheless, some researchers [84, 85] have also suggested that it is the generation of ceramic-polymer grain boundaries that provides a "fast channel" for ion transportation.

Reactive or conducting fillers have been used in CPE systems. Unlike inert fillers, these types of fillers directly participate in the conduction process. Lithium nitride (Li_3N) is one of the examples. When mixed into $\text{Li}^+/\text{P}(\text{EO})_{12}$, the ionic conductivity is as high as 10^{-4} - 10^{-3} Scm^{-1} at room temperature [76]. Nevertheless, this type of CPE system is however electrochemically unstable and fragile. Other examples of reactive fillers are NASICON ($\text{Na}_{3.2}\text{Zr}_2\text{Si}_{2.2}\text{P}_{0.8}\text{O}_{12}$), sulfide glass ($1.2\text{Li}_2\text{S}$ - 1.6LiI - B_2S_3) [3, 56] and $\text{Li}_{1.3}\text{Al}_{0.3}\text{Ti}_{1.7}(\text{PO}_4)_3$ [5, 77] etc.

In the 90's, the "nano" fever hit the field of CPE. Instead of micron size fillers, scientists have undertook fillers of nano-size regime. Krawiec and co-workers [78] have studied the size effect of Al_2O_3 fillers on the properties of CPEs. They found that the glass transition temperature (T_g) and crystallinity of the CPE are independent of the size of Al_2O_3 , but the ionic conductivity as well as the interface stability of the CPE are higher for the nano-sized filler compared to the system utilizing micron-sized fillers.

Apart from the above mentioned ceramic and glass-type fillers, other fillers have also been applied in CPE systems. Semiconductor oxides and sulfides, modified and un-modified clays, zeolites and silica with various structures can be found in literature. These are listed in Table 2.3. In most of the CPE systems, the electrical conduction is nearly pure ionic arising from the salt's migration. However, Chandra et al. [79, 80] have reported that the addition of semiconducting sulfide fillers (viz. PbS, CdS, $PbxCd_{1-x}S$, CuS) also introduce another type of electrical conduction to the system, i.e. the electronic conduction apart from the ionic conduction.

Table 2.3: Solid fillers utilized in CPE systems.

Type	Filler entity	Reference
Ceramic	Al_2O_3	[75, 78, 81]
	$LiAlO_2$	[81]
	TiO_2	[82]
	SiO_2	[83]
Metal oxides	SnO_2	[84]
	MgO	[85]
	$SrBi_4Ti_4O_{15}$	[86]
	ZnO	[87]
	Fe_3O_4	[88]
	CdO	[89]
	CuO	[90]
	CeO_2	[91]
Metal sulfides	CdS	[79]
	PbS	[79]
	$PbxCd_{1-x}S$	[79]
	CuS	[80]
	Bi_2S_3	[92]
Clay	Organic-montmorillonite (MMT)	[93]
Zeolite	MCM-41	[87]
	SBA-15	[87]
	ZSM-5	[94]

2.1.3.3 Iodine dopant

Iodine (I_2) is usually added as dopant to the PE system of metal iodide (MI)-polymer to further tailor the properties of the ensued PEs. The combination of I_2 -MI-polymer is suitable for dye-sensitized solar cell (DSSC) applications. The I_2

easily combines with I^- to form I_3^- and this produces a redox couple of I^-/I_3^- in the system which facilitates the electron transfer to the dye in the DSSC. The equations for the redox process are as follows [95, 96]:



Numerous I_2 -MI-polymer systems have been explored, including I_2 -NaI-poly(acrylonitrile-co-styrene) [96], I_2 -KI-PEO-succinonitrile [97], I_2 -MgI₂-polyethylene glycol [41], I_2 -LiI-agarose [98] and the likes. To prepare I_2 -MI-polymer PEs, I_2 is mixed together with MI and the polymer solution under vigorous stirring followed by casting and drying process. Another method is to soak the polymer membrane in the mixture of I_2 and MI electrolyte solution followed by drying.

2.2 Application of polymer electrolytes

As a new class of solid ionic material, PE has been adopted in a wide range of energy production and storage applications. PE is one of the key components in the assembly of cells, capacitors, electrochemical devices and sensors. Generally, PE functions as a separator between the electrodes and allows the transportation of ions. The potential applications of PE and some of the examples are shown in Table 2.4.

Table 2.4: Potential applications of PE

Application	Example of PE	Reference
Batteries	Li ⁺ /P(VDF-HFP)	99, 100
Fuel cells	H ⁺ /Nafion [®] , H ⁺ /SPEEK, H ⁺ /PVDF	101, 102
Photoelectrochemical cells	Li ⁺ /PEDOT	103-105
supercapacitors	Li ⁺ /PEO, K ⁺ /PVA, Li ⁺ /PU, Li ⁺ /PVDF, Li ⁺ /glycerol/chitosan-starch	106-113
Electrochromic devices	Li ⁺ /P(EO) ₈	3, 56
Sensors and actuators	Rb ⁺ /PEO, Li ⁺ /P(VDF-HFP)	114, 115

2.3 Epoxidized natural rubber

Chemical modification is a common method to alter the physical properties of natural rubber (NR) which in turn diversify its applications. Epoxidation is a reaction where the isoprene units are converted into epoxide group using organic peracids [117]. For NR, this is shown in Figure 2.2.

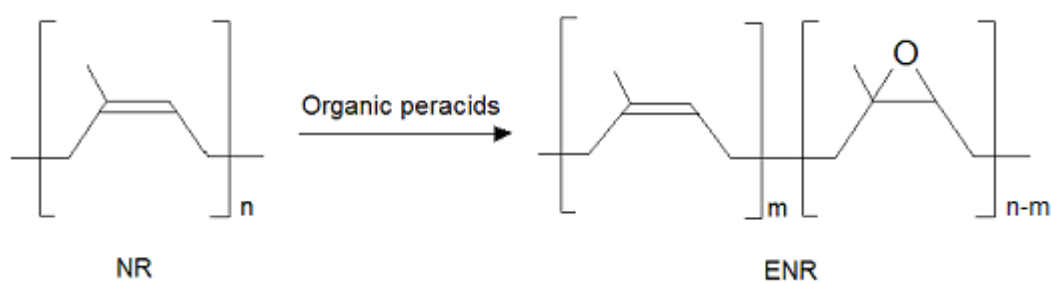


Figure 2.2: Epoxidation of natural rubber (NR) [117].

Introduction of this polar epoxide group into the NR structure has increased the tensile strength, fatigue properties and improved the oil, solvent and wear resistance. Unfortunately, it also resulted in a reduction of resilience and gas permeability [117].

2.3.1 ENR blends

Blending two or more different polymers to form a new material with desired properties is a common practice for many decades. This method is easy, cheap and less time consuming [118]. In this regard, epoxidized natural rubber (ENR) has been blended with a number of polymers to further tailor its physical properties and processability. Both reactive and non-reactive ENR blends can be found in literatures. The examples are polychloroprene rubber (CR)/ENR [119], Nylon-12/ENR [120], poly(3-hydroxybutyrate) (PHB)/ENR [121], poly(ethylene-co-acrylic acid) (PEA)/ENR [118], poly(3-hydroxybutyrate-co-3-hydroxyvalerate) (PHBV)/ENR [122], poly(vinyl chloride) (PVC)/ENR [123], SMR L natural rubber/ENR [124], styrene butadiene rubber (SBR)/ENR [125] and the likes. These blends are said to exhibit better mechanical, thermal, rheological properties etc. as compared to their parent polymers. However, in most of the cases, this claim is true or only applicable to certain blend compositions. Besides, the blending condition is also a crucial factor to determine the performance of the produced blend.

2.3.2 Inorganic/ENR composites

Early work on inorganic/ENR composites is mainly based on silica reinforced ENR composite in relation to tyre application. Besides the commercial silica fillers, the use of silica fillers obtained from rice husk ash has also been reported [126]. It is found that the vulcanisate and reinforcement properties of silica/ENR composites are comparable to conventional carbon black filled NR compounds [127]. Other types of reinforced fillers like clay [128] and modified silica-aluminium-carbon (MSAC) [129] are also incorporated into ENR to enhance its physico-mechanical properties.

Recently, metal nanoparticles, viz. Au⁰, Pt⁰, Ag⁰ have been incorporated into ENR matrix [130, 131]. In these metal/ENR nanocomposites, the ENR matrix

exerts stabilization effect on the metal particles while the **later** exert interesting optical, electrical and thermal properties to the nanocomposites. Thus, the metal/ENR nanocomposites are potential candidate for electrical conductive adhesives (ECA), thermal interface materials (TIM) and so forth.

2.3.3 ENR-based polymer electrolytes

Idris and co-workers [49, 50] were the first group who explore the possible usage of ENR in PEs. A series of unplasticized and EC/PC-plasticized ENR PEs that exhibited ionic conductivities in the range of 10^{-6} - 10^{-3} Scm^{-1} at ambient temperatures were prepared. This group continued to study the effect of the addition of PEO on the electrical and thermal properties in PEs. Following this, a group of Japanese researchers [132-134] also showed their interest in ENR-based PEs in a different aspect. They were concerned with the effect of protein and epoxidation level of ENR towards the thermal and electrical properties of ENR/bis(trifluoromethane sulfonyl)imide (LiTFSI) PEs. Later on, several other studies based on ENR PEs ensued. These include the investigation on the effect of wt% of EC/PC mixture in the system of ENR/lithium imide ($\text{LiN}(\text{CF}_3\text{SO}_2)_2$) [135]. While others blended the ENR with polymers like PEO [136-138], PVDF [139], PMMA [140, 141] and PVC [142-146] to form ternary (without plasticizer) or quaternary (with plasticizer) PE systems. In 2008, Mohamed et al. [147] fabricated the lithium-air primary cells utilizing ENR-based PEs and reported the electrochemical properties. This study proved the capability of ENR with respect to cell applications. The incorporation of inorganic filler viz. ZnO particles into the ENR-based PE has also been reported recently [148].

2.4 Iron oxides

Iron oxides are among the most abundant compounds found in nature. They exist in the atmosphere, pedosphere, biosphere, hydrosphere and

lithosphere [149] in various types of structure or compositions. There are 16 types of iron oxides (Table 2.5) including those composed of Fe with O and/or OH according to the classification by Cornell and Schwertmann [149].

Table 2.5: Various types of iron oxides

Group	Examples
Oxide-hydroxides and hydroxides	Goethite, g-FeOOH
	Lepidocrocite, b-FeOOH
	Akaganeite, a-FeOOH
	Schwertmannite, $\text{Fe}_{16}\text{O}_{16}(\text{OH})_y(\text{SO}_4)_z \cdot n \text{H}_2\text{O}$
	d-FeOOH
	Feroxyhyte, d'-FeOOH
	High pressure FeOOH
	Ferrihydrite, $\text{Fe}_5\text{HO}_8 \cdot 4 \text{H}_2\text{O}$
	Bernalite, $\text{Fe}(\text{OH})_3$
	$\text{Fe}(\text{OH})_2$
Green rusts, $\text{Fe}_x^{\text{III}}\text{Fe}_y^{\text{II}}(\text{OH})_{3x+2-z}(\text{A}^-)_z$; A = Cl^- ; 0.5SO_4^{2-}	
Oxides	Hematite, a- Fe_2O_3
	Magnetite, Fe_3O_4 ($\text{Fe}^{\text{II}}\text{Fe}_2^{\text{III}}\text{O}_4$)
	Maghemite, g- Fe_2O_3
	b- Fe_2O_3
	e- Fe_2O_3
Wustite, FeO	

2.4.1 Magnetite

Magnetite (Fe_3O_4) is known to be of low toxicity and biocompatible and comprises of 72.36 % Fe and 27.64 % O. It differs from most other iron oxides in that it contains both ferrous (Fe^{2+}) and ferric (Fe^{3+}) ions. Fe_3O_4 has an inverse spinel structure with Fe^{2+} located at the octahedral (B) site and Fe^{3+} situated at both the tetrahedral (A) and octahedral sites (B) [149]. The hole/electron(s) can easily migrate between the Fe^{2+} and Fe^{3+} ions in the octahedral sites of Fe_3O_4 , making the Fe_3O_4 a good semiconductor. The conductivity of Fe_3O_4 is almost

metallic and it falls in the range of 10^2 - 10^3 W^1cm^{-1} [149]. At room temperature, the electron spins of Fe_3O_4 on A and B sites are anti-parallel and the magnitudes of these opposite spins are unequal, therefore bulk Fe_3O_4 is ferromagnetic. Nevertheless, under a sufficient thermal energy, Fe_3O_4 can be transformed into a paramagnetic material [149]. Furthermore, the Fe_3O_4 particle with size below 15 nm exhibits superparamagnetism [149].

In the recent decade, Fe_3O_4 /polymer composites have become one of the emerging classes of advanced materials. These composites are said to offer improved performance and functionalities adopted from either or both of the respective components. Generally, Fe_3O_4 /polymer composites can be divided into 2 types: (1) Fe_3O_4 coated polymer composites (where Fe_3O_4 is the continuous phase) and (2) Fe_3O_4 incorporated polymer composites (where polymer is the continuous phase). In another word, the polymer functions as binder and matrix in type (1) and (2) respectively. This is illustrated in Figure 2.3.

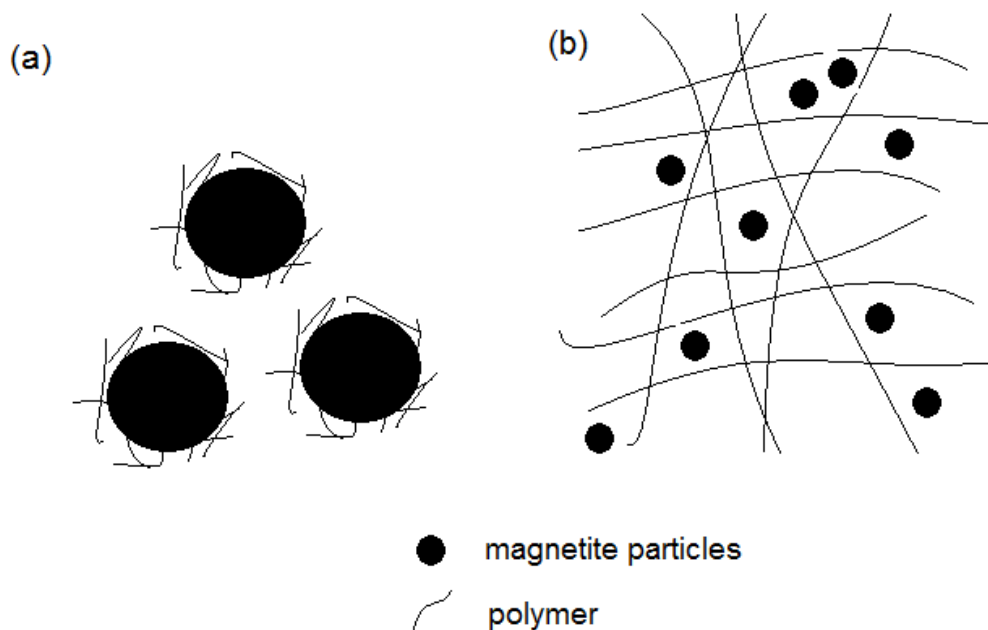


Figure 2.3: (a) Fe_3O_4 coated- and (b) Fe_3O_4 incorporated polymer composites.

Depending on the applications, Fe₃O₄ particles can be combined with any suitable polymer of desired properties. For example, Fe₃O₄ particles has been incorporated into non-toxic, biocompatible and biodegradable polymers such as poly(D,L-lactide) (PDLLA) [150], alginic acid [151], L-lysine [152], PVP [153] and poly(lactic-co-glycolic acid) (PLGA) [154] for biomedical applications. Other polymers such as polyurethane (PU) [155], polyaniline (PANI) [156], polypyrrole (Ppy) [157], PEO [158] and natural rubber [159], have also been used to prepare the respective Fe₃O₄/polymer composites. These composites have potential use in other fields such as electronic and magnetic devices.

2.4.2 Applications of magnetite

The applications of magnetite cover numerous fields. Table 2.6 shows some of the examples.

Table 2.6: Applications of magnetite.

Field	Role	Applications	References
Industry	Colorants/ pigments	Paints, coating and construction materials	149
	Catalysts	Haber process, water gas shift reaction and Fisher-Tropsch synthesis	149
Biomedical	Contrasting agent	Magnetic resonance imaging (MRI)	160
	Heating mediator	Hyperthermia treatment and controlled drug release delivery system	161, 162
Communication	Wave absorber	Wireless communication technologies	159, 163-166
Electronic	Electrode materials	Supercapacitors and lithium batteries	167-170
	Conducting materials	Flow sensor, humidity sensor, chemiluminescence sensor and conductometric immunosensor	171-175
Environment	Absorber	Waste water treatment	176-180

2.5 Kinetic Analyses

In the study of solid state kinetics, numerous methods including Arrhenius have been proposed and applied in the past. Nevertheless, the model-free Kissinger and Flynn-Wall-Ozawa (FWO) methods and the model-fitting Coats-Redfern (CR) method are the most common method employed in the degradation study.

2.5.1 Theoretical background

The kinetic parameters like activation energy (E) for a thermal degradation reaction of a material can be determined using TG analyses under isothermal or non-isothermal conditions. In TG analyses, the reaction rate can be defined as the variation in degree of conversion (a) versus time or temperature. a is calculated based on mass lost using equation (2.4) [181]:

$$a = \frac{m_i - m_t}{m_i - m_{\infty}} \quad (2.4)$$

The m_i , m_t and m_{∞} represents the initial mass, mass at temperature t and final mass for a sample. The rate of conversion (da/dt) in thermal degradation is a function of temperature dependent rate constant (k) and a temperature independent function of conversion [f(a)], thus it is expressed as in equation (2.5) [181, 182]:

$$\frac{da}{dt} = kf(a) \quad (2.5)$$

k can also be represented by Arrhenius equation (2.6) where A, E, R and T are the pre-exponential factor, activation energy, gas constant and absolute temperature respectively.

$$k = Ae^{\frac{-E}{RT}} \quad (2.6)$$

And for a constant heating rate (b), it is defined by equation (2.7):

$$\frac{b}{dT} = \frac{1}{dt} \quad (2.7)$$

Substitution of equation (2.6) and (2.7) into equation (2.5), gives the common fundamental equation (2.8) based on TG data.

$$\frac{da}{dT} = \frac{A}{b} e^{\frac{-E}{RT}} f(a) \quad (2.8)$$

2.5.2 Isoconversional methods

Kissinger and Flynn-Wall-Ozawa (FWO) methods are often employed in the kinetic analyses of the non-isothermal degradation of ENR-based PEs. Both methods are applied without the precise knowledge of the kinetic model/ reaction mechanism in advance. These two methods are derived from equation (2.8) using differential or integral approaches.

2.5.2.1 Kissinger method

The Kissinger equation (2.9) is shown as below. Here, b is the heating rate, T_p is the temperature for maximum degradation rate determined from DTG curve of (mass loss versus temperature) thermogram, E_d is the degradation activation energy, A is the pre-exponential factor, R is the gas constant and T is the absolute temperature. The respective E_d values are obtained from the slope of the plots of $-\ln b/T_p^2$ against $1/T_p$ [182, 183].

$$-\ln \frac{b}{T_p^2} = \frac{E_d}{RT_p} - \ln \frac{AR}{E_d} \quad (2.9)$$

2.5.2.2 Flynn-Wall-Ozawa method

Integration of equation (2.8) using the Doyle approximation gives the FWO equation (2.10) [182, 185]. The b , E_d , R , T and A represent similar meanings as in Kissinger method and the $g(a)$ represents the integral function of conversion. A straight line is obtained from the plot of $\log b$ against $1/T$ at a constant a . Thus the value of slope is equal to $0.4567/(E_dR)$.

$$\log b = \frac{-0.4567E_d}{RT} - 2.315 + \log \frac{AE_d}{R} - \log g(a) \quad (2.10)$$

2.5.3 Model-fitting methods

2.5.3.1 Coats and Redfern method

CR is a model-fitting method based on single heating rate. This is shown in equation (2.11) [186-188]:

$$\ln \frac{g(a)}{T^2} = \ln \frac{AR}{bE_d} - \frac{E_d}{RT} \quad (2.11)$$

The $g(a)$ has different expressions for different types of mechanisms and kinetic models. These are tabulated in Table 2.6. E_d is calculated from the slope of the straight line of plot $\ln g(a)/T^2$ versus $1/T$. The E_d values for different $g(a)$ is compared to those obtained from isoconversional methods.